1. Report No. FHWA/TX-08/0-5310-1	2. Government Accession No.	3. Recipient's Catalog No.
4. Title and Subtitle Development of a Scanning Laser System for Measuring Seal Coat Quality		5. Report Date March 2007 6. Performing Organization Code
7. Author(s) Richard Liu, Wei Sun, Yuanhang Chen, Pankaj Chopra, Jing Li, and Xuemin Chen		8. Performing Organization Report No. Report 0-5310-1
9. Performing Organization Name and Address Department of Electrical and Computer Engineering University of Houston 4800 Calhoun Rd. Houston, TX 77204-4005		10. Work Unit No. 11. Contract or Grant No. Project 0-5310
12. Sponsoring Agency Name and Address Texas Department of Transportation Research and Technology Implementation Office P.O. Box 5080 Austin, TX 78763-5080		13. Type of Report and Period Covered Technical Report Sep 1, 2005 – Aug 31, 2006 14. Sponsoring Agency Code
15. Supplementary Notes Project performed in cooperation with the Texas Department of Transportation and the Federal Highway Administration. URL: http://subsurface.ee.uh.edu/documents/0-5239.pdf		

16. Abstract:

In this project, a 3-D laser scanning imaging system based on auto-synchronized scanning is developed for evaluation of seal coat quality. Compared to the classical triangulation technique, this approach does not sacrifice the system resolution for the large field of view. To achieve high-speed measurement, a PSD (Position Sensitive Detector) is used in the prototype system instead of a CCD (Charge Couple Device), which is usually used in the common imaging system. By using a galvanometer scanner, the system can scan up to100 lines per second. Compared to the previous mechanical scanning device, which gives two scan lines per second, the new system is more suitable for highway speed measurement. The system is tested both in the lab with different distances. The result shows the great potential of this system to be applied in pavement survey.

17. Key Words MEMS Technology, Nanotechnology, Transportation Engineering, Sensor Application, Wireless Sensor Network, Smart Material	18. Distribution Statement No restrictions. This document is available to the public through National Technical Information Service, Springfield, Virginia, 22161, www.ntis.gov

19. Security Classif. (of this report) Unclassified	20. Security Classif. (of this page) Unclassified	21. No. of Pages 36	22. Price

Development of a Scanning Laser System for Measuring Seal Coat Quality

by

Richard Liu, Wei Sun, Yuanhang Chen, Pankaj Chopra, Jing Li, and Xuemin Chen

Research Report 0-5310-1

Project Number: 0-5310
Project title: The Evaluation of a System for Measuring Seal Coat Quality

Performed in Cooperation with the
Texas Department of Transportation and the Federal Highway Administration

by the

Subsurface Sensing Laboratory
Department of Electrical and Computer Engineering
University of Houston

March 2007

DISCLAIMERS

The contents of this report reflect the views of the authors, who are responsible for the facts and the accuracy of the data presented herein. The contents do not necessarily reflect the official view or policies of the Federal Highway Administration (FHWA) or the Texas Department of Transportation (TxDOT). This report does not constitute a standard, specification, or regulation.

University of Houston
4800 Calhoun Rd.
Houston, TX 77204

ACKNOWLEGMENTS

We greatly appreciate the financial support from the Texas Department of Transportation that made this project possible. The support of the project director and the project coordinator are also very much appreciated.

Table of Contents

List of Figures

CHAPTER 1: INTRODUCTION

1.1 Background and overview

Seal coating is a common preventive maintenance activity in Texas performed by most cities, counties and rural districts. It involves spraying asphalt cement on the surface of an existing pavement followed by the application of a cover of aggregate. The asphalt cement is usually emulsified (suspended in water) to allow for the application without the use of extreme heat. The cover aggregate is normally either naturally occurring gravel or crushed aggregate such as granite, quartzite or trap rock (basalt).

The primary reason to seal coat an asphalt pavement is to protect the pavement from the deteriorating effects of sun and water. When an asphalt pavement is exposed to sun, wind and water, the asphalt hardens, or oxidizes. This causes the pavement to become more brittle. As a result, the pavement will develop cracking because it is unable to bend and flex when exposed to traffic and temperature changes. A seal coat combats this situation by providing a waterproof membrane which not only slows down the oxidation process but also helps the pavement to shed water, preventing it from entering the base material.

A secondary benefit of seal coating is an increase in surface friction. This is accomplished by the additional texture the cover aggregate adds to the pavement. With time, traffic begins to wear the fine material from an asphalt pavement surface. These results in a condition referred to as raveling. When enough of the fine material is worn off the pavement surface, traffic is driving mostly on the course aggregate. As these aggregate particles begin to become smooth and polished, the roadway may become slippery. Highway geometric design is driven by the ability to stop of the vehicles (stopping sight distance), a function of pavement friction factors, and the availability of suitable side friction factors around curves. A seal coat increases the pavement texture and increases the surface friction properties. In order for aggregate particles to remain on the roadway, they need to have approximately 70 percent of their height embedded into the residual asphalt, as shown in Figure 1-1.

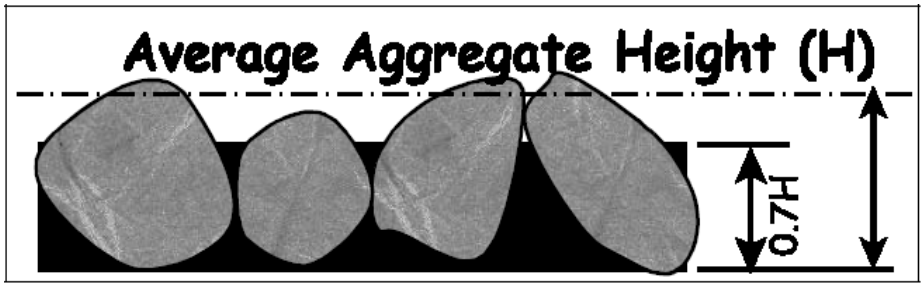

Figure 1-1 Proper embedment (~70%) into the residual asphalt.

The primary defects in seal coats and surface treatments are loss of aggregate, poor adhesion, streaking, and flushing. Examples of some of these pavement conditions are shown in Figures 1-2 to 1-6.

Figure 1-2 Too much aggregate (no binder is visible)

Figure 1-3 Streaking caused by incorrect spray bar height.

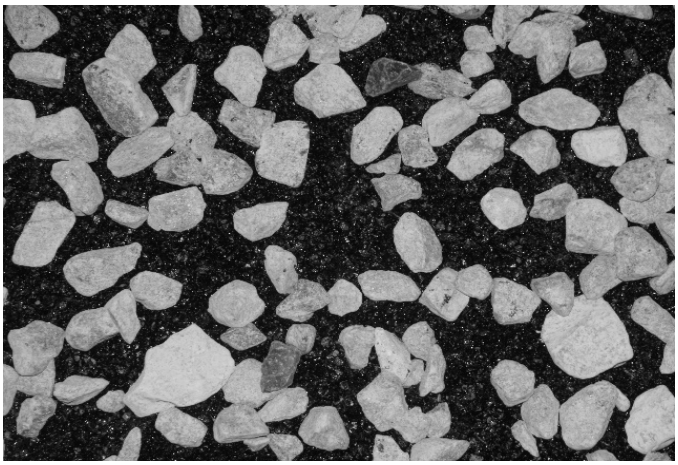

Figure 1-4 Shelled seal coat surface: not enough binder.

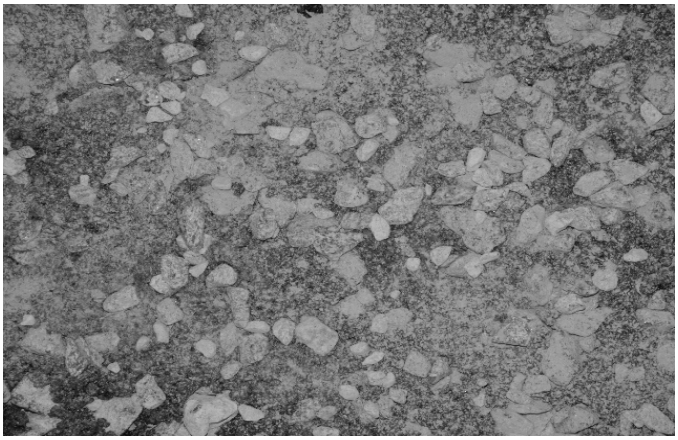

Figure 1-5 Flushed seal coat surface.

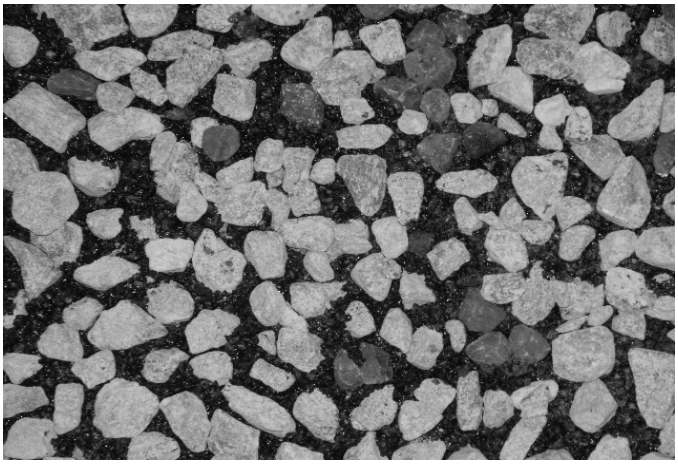

Figure 1-6 Correct amount of binder (binder has risen to top of chips)

Among the several distress types observed with seal coat surfaces, two of those—flushing and shelling were the most common ones (Benson and Galloway, 1953; Holmgreen et al., 1985). Flushing (also called bleeding) is characterized by the excessive embedment of aggregate into the asphalt binder and a loss of skid resistance that is caused by the extra binder on the surface. In other words, a flushed surface has a smooth and slick appearance where the aggregates are less visible. Such distress is usually observed on the wheel paths where repetitive load cycle of tires cause subsequent embedment of aggregates. Flushing may be exacerbated by high binder application rates as well as with high surface temperatures during the day.

Shelling (also called raveling), on the other hand, is the loss of aggregate from the pavement's surface. Such pavements have a very irregular appearance since the surface is not completely covered by the aggregate. This type of distress is generally observed on the centerline and between the wheel paths of the pavement. Shelling occurs when the desired bond between the aggregate and binder fails. Low binder application rates, inadequate rolling, cool weather construction, and incompatible binder and aggregate types are common factors that might lead to shelling.

Current methods to determine performance indicators on seal coats such as aggregate loss and flushing are very subjective. For example, the loose unit weight (W) is determined according to ASTM C 29 and is needed to calculate the voids in the aggregate in a loose condition. This is time consuming and labor intense. Consequently, there is a need to develop an accurate and rapid method to quantify the defects that may occur in the seal coat and the level of severity of these defects.

In this project, three instruments that will be evaluated to determine whether or not the data can be used to locate and measure loss of aggregate and flushing during annual PMIS data collection efforts. These instruments are the FMCW radar, texture laser and the auto-synchronized scanning laser devices. The texture laser and auto-synchronized scanning laser can measure the pavement profile with high accuracy. It has great potential to quantify seal coat surface.

CHAPTER 2: FILED EVALUATION METHODS

There are several traditional and emerging methods to detect and quantify texture, so that a quality control/quality assurance program can be built into the design and construction of pavements seal coat. Following is a description of those methods.

2.1 Sand Patch Method

The Sand Patch test procedure is described in ASTM E965. It uses a volumetric approach for measuring pavement macrotexture. A known volume of glass beads is spread evenly over the pavement surface to form a circle, thus filling the surface voids as shown in Figure 2-1. The diameter of the circle is measured on four axes and the values averaged. This value is used to calculate the mean texture depth (MTD).

Figure 2-1 Sand patch testing

2.2 Outflow Meter

This is an indirect measure of texture as shown in Figure 2-2 and Figure 2-3. A cylinder with rubber seals on its lower end is placed on the surface and loaded by weights to assure good contact. An electric timer is connected to probes inside the cylinder. The

cylinder is filled with water. To start the test, the plunger sealing of the outlet is lifted and the water escapes between the rubber seals and the pavement surface. The time for the water to escape is a measure of texture. Deep textured surfaces will allow fast escape of water; i.e., the outflow time for deep textured surfaces is shorter than the outflow time for shallow textured surfaces.

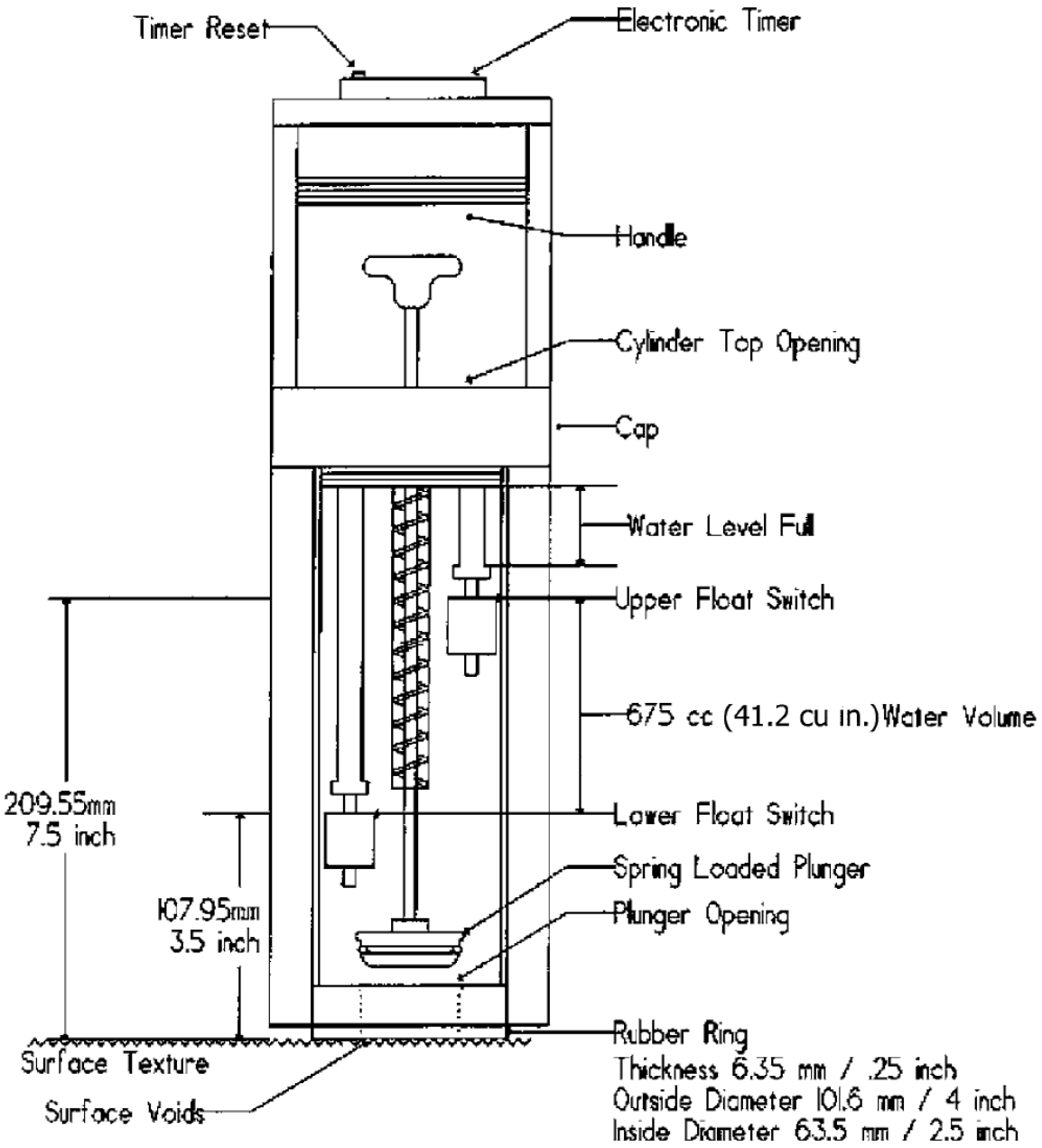

Figure 2-2 Outflow meter

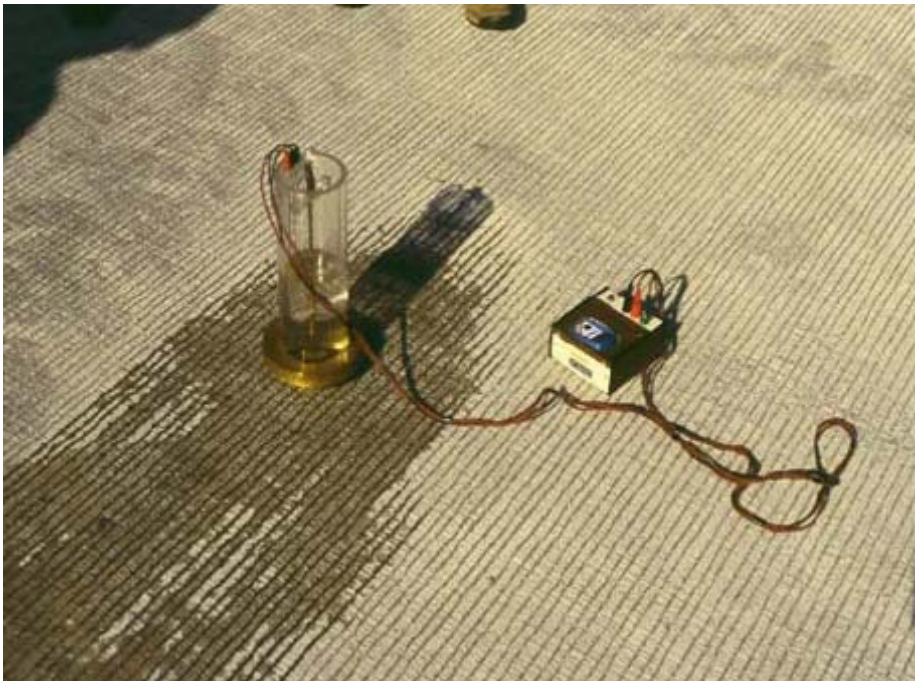

Figure 2-3 Outflow meter testing

2.3 Laser Surface Texture Measurement

Over the past twenty years the use of laser technology to define surface texture has been gaining wide popularity. The basic concept of the measurement system is illustrated in Figure 2-4. Using mathematical algorithms the distance to the surface at a discrete point is obtained. The measurements are conducted very rapidly as the vehicle drives along the pavement enabling measurements at points that can be typically separated by 1mm (1/25-inch) defining a surface profile as illustrated in Figure 2-5.

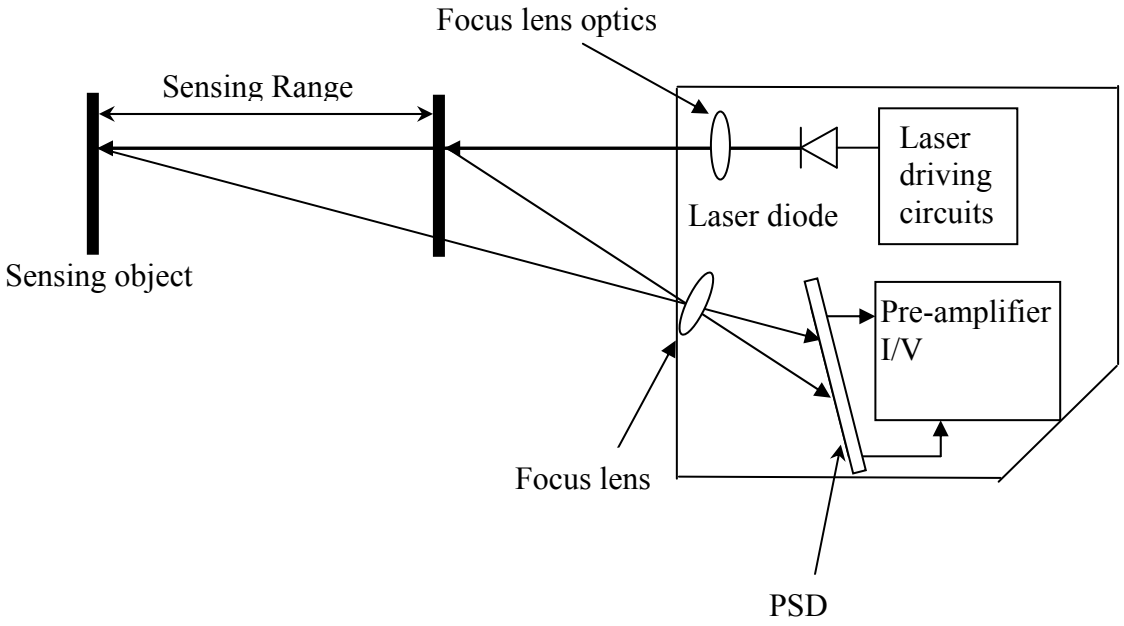

Figure 2-4 Laser-based triangulation system

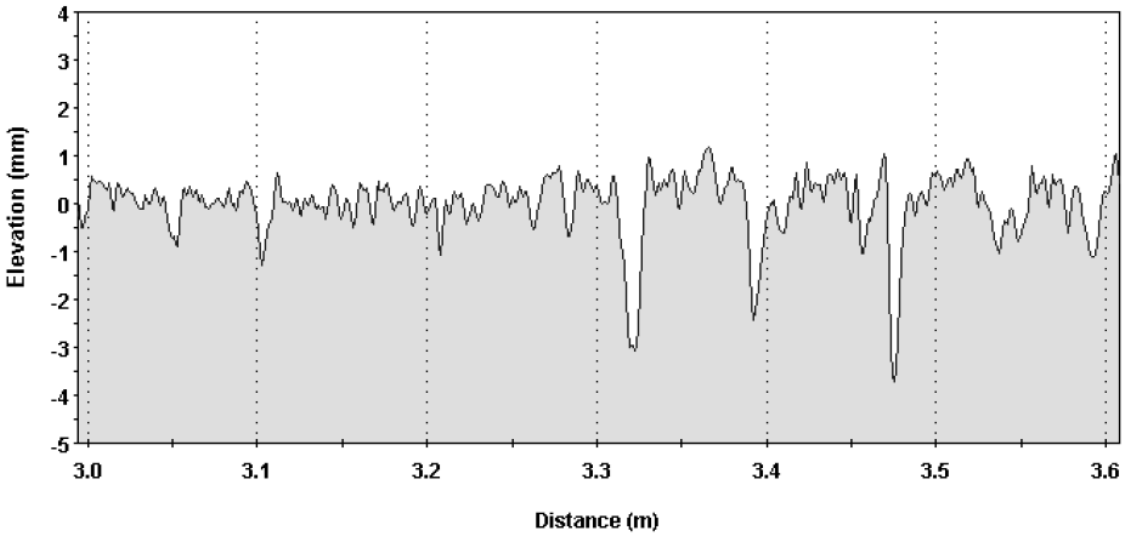

Figure 2-5 Example of laser surface texture measurement over a 0.6m length

The assessment of texture with vehicle-mounted laser measuring devices is shown in Figure 2-6.

Figure 2-6 Vehicle-mounted laser measuring devices developed by University of Houston

CHAPTER 3: SCANNING LASER SYSTEM DESIGN AND SPECIFICATIONS

3.1 Principle Review of laser Triangulation

The triangulation method (Manuel 1996, Wiese 1989) is the most commonly used approach in modern industry for applications requiring an operating range that is less than 10 meters. Currently, there are a limited number of triangulation-based sensors available commercially for the ranges between 2 meters and 10 meters. The fundamental geometrical principle of optical triangulation is shown in Figure 3-1. The shape of the triangle can be determined by knowing two angles (α and $\Delta\beta$) of the triangle to its base (baseline d). Measuring the change $\Delta\beta$ can evaluate the incremental change of distance Δz. To measure a profile, one needs to scan the spot. Figure 3-2 shows the basic geometrical principle of laser scanning triangulation. The laser beam is deflected by a scanning mirror and scans over the object. A camera, constituted of lens and a position sensitive photodetector, measures the location of the image of the illuminated point on the object.

So far, the laser-optic triangulation has been widely used in many applications of both profiling and range measurement for its advantages of low cost, simplicity, robustness and good resolution. Although having those advantages, the classical triangulation technique has some limitations. To show the limitations of triangulation, people approximated the measurement uncertainty of error in depth z by the law of propagation of errors. The measurement uncertainty in z is inversely proportional to both the effective focal length f of the lens and the separation distance d between the laser and the detector, but directly proportional to the square of the distance. Unfortunately, f and d can't be made as large as desired. The separation distance d is limited mainly by the mechanical structure of the optical setup (stability of the whole system decreases as d increases) and by shadow effects (self occlusion problems increase with d) which is shown in Figure 3-3. The focal length f is limited by the issue of the field of view Φ_x. Both of the uncertainty in z and the field of view Φ_x are inversely proportional to the f, which means

there is always a compromise consideration between the accuracy and the field of view in conventional triangulation set up (Blais et al, 1988).

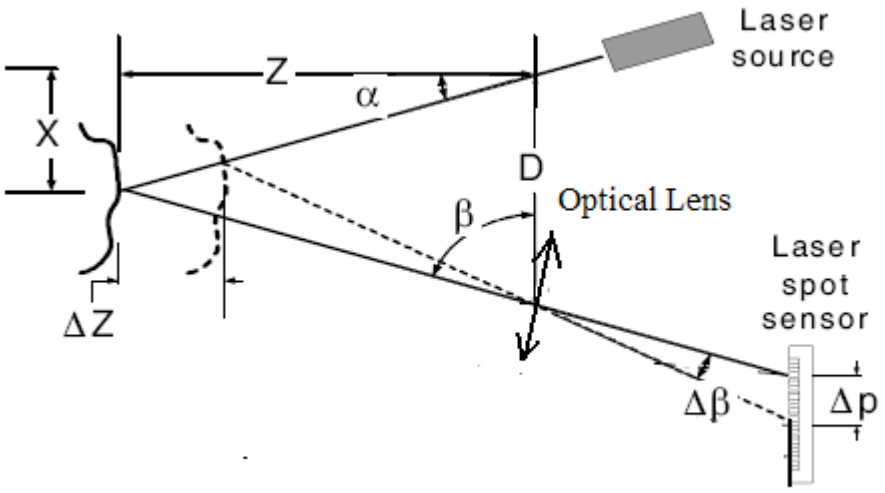

Figure 3-1 Geometrical Principle of Triangulation

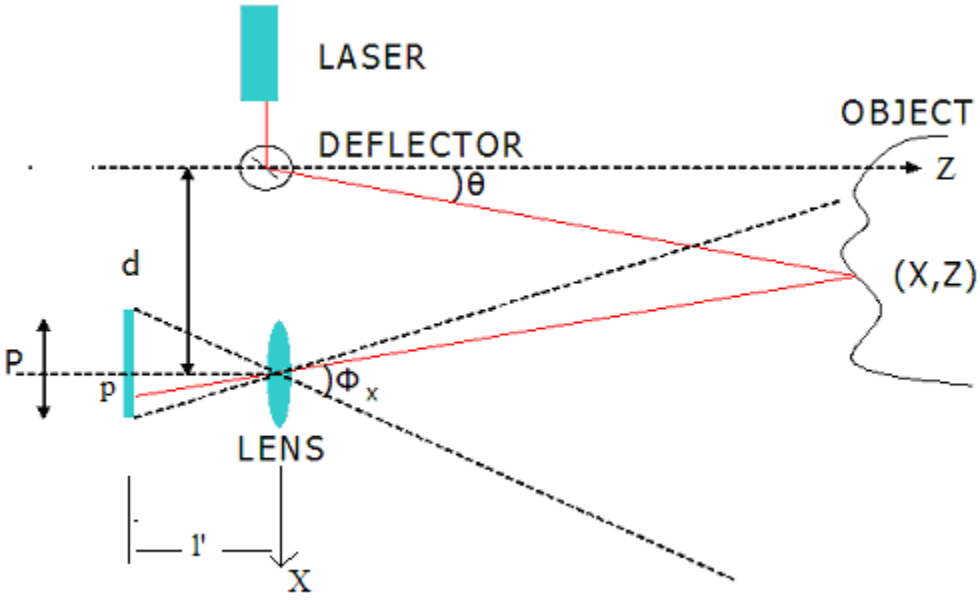

Figure 3-2 Geometrical Principle of Laser Scanning Triangulation

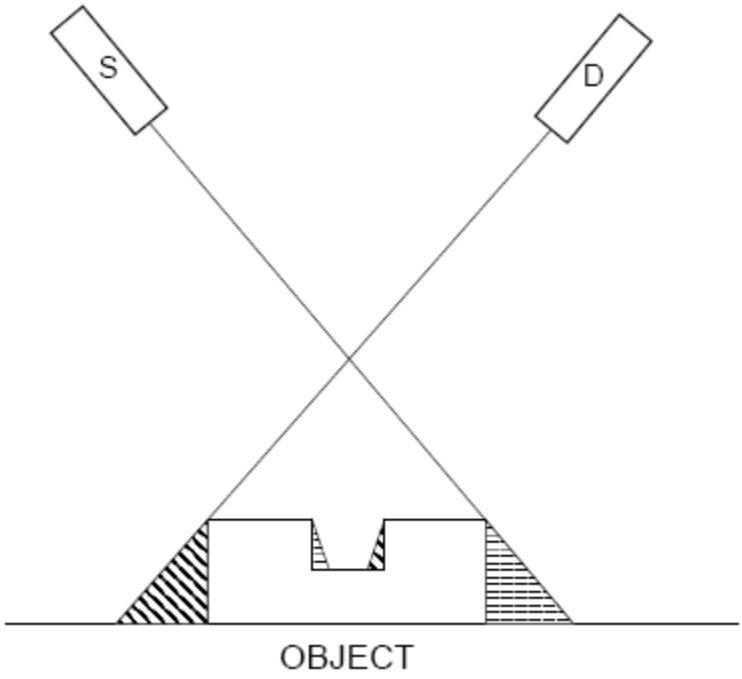

Figure 3-3 Shadow Effects

To alleviate the problems associated with the classical triangulation, we introduce an innovative approach called auto-synchronized scanning mechanism that allows a very large field of view without compromising the performance of the system.

3.2 Auto-Synchronized Laser Scanning Principle

3.2.1 Optical configuration of auto-synchronized scanning laser principle

The innovative approach of auto-synchronized scanning technique was presented (Rioux 1994). The basic idea is to synchronize the projection of a light spot with its detection. Figure 3-4 shows the optical configuration of the auto-synchronized scanning laser system. A double-sided coated mirror is used as a scanning device. One side of the mirror is used to deflect the laser beam. The other side collects the reflected light from the scene. By using this configuration, the instantaneous field of view follows the laser

spot as it scans over the scene, which means the focal length of lens f is therefore related only to the desired depth of field or measurement range.

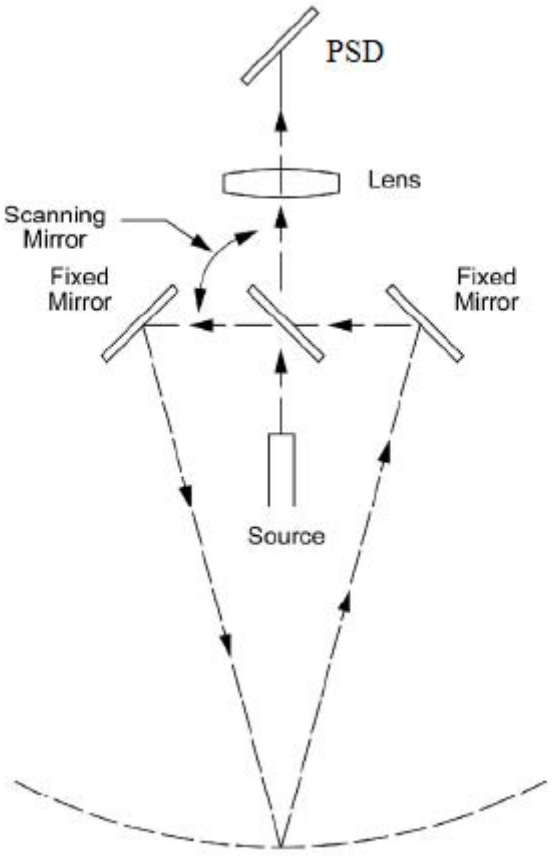

Figure 3-4 Optical Configuration of Auto-Synchronized Laser Scanning

3.2.2 Algorithm of auto-synchronized laser scanning technique

Figure 3-5 shows the geometry used for the triangulation where the projection and collection axes have been unfolded. The synchronized geometry shows that, at a spot position p=0 (point A); the acute angle between the projection and collection paths is equal to a constant γ. So we can deduce all the other angles from this. Based on the triangulation geometry, we can prove two triangles OAC-OED are similar, same as triangles OBC-OFD. From these, we can deduce the following relation.

$$\frac{R_p(\theta) - R_0(\theta)}{R_p(\theta) - R_{-\infty}(\theta)} = \frac{p}{P_\infty} \tag{2}$$

where p is the image position on the detector (detection axis), PSD, of the laser spot and for a given deflected angle θ, $R_p(\theta)$ is the distance $R(\theta)$ along the projection axis corresponding to p. $R_{-\infty}(\theta)$ is the location of the vanishing point on the projection axis, and $R_0(\theta)$ is the location corresponding to p=0. P_∞ is the location on the position detector of the vanishing point on the detection axis and is described as:

$$P_\infty = f_0 \frac{\sin(\gamma)}{\cos(\beta - \gamma)} = \frac{(f_0 - f)}{\sin(\beta)} \tag{3}$$

where f is the focal length of the lens, f_0 is the effective distance of the position detector to the imaging lens, β is the tilt angle of the position detector and γ is the triangulation angle.

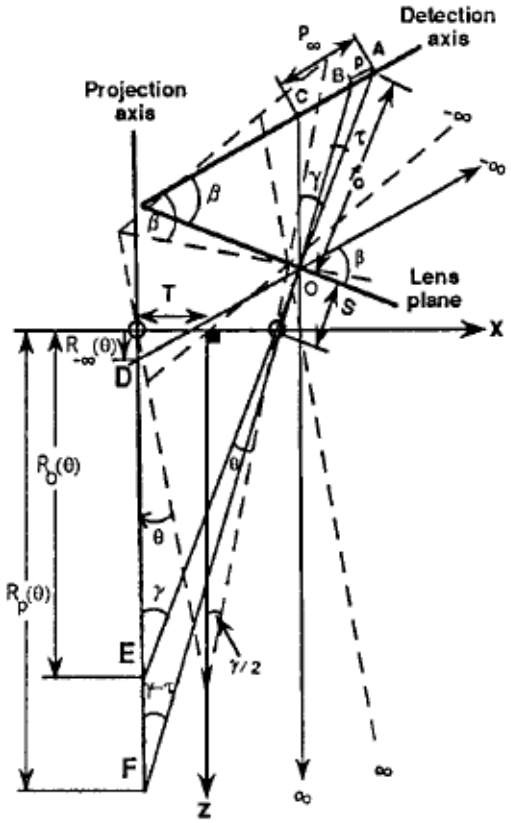

Figure 3-5 Unfold Geometry of Auto-synchronized Laser Scanning Triangulation

The transformation of above equation to an (X,Z) representation is computed from the fact that two points D and E and a third point F belong to the same straight line if the vectors DE and DF are linearly dependent. Hence,

$$\frac{X_p(\theta)-X_0(\theta)}{X_p(\theta)-X_{-\infty}(\theta)}=\frac{Z_p(\theta)-Z_0(\theta)}{Z_p(\theta)-Z_{-\infty}(\theta)}=\frac{p}{P_\infty} \tag{4}$$

The above equations are decomposable in both orthogonal directions, i.e.

$$x(p,\theta)=X_{-\infty}(\theta)+P_\infty\frac{X_0(\theta)-X_{-\infty}(\theta)}{P_\infty-p} \tag{5}$$

$$z(p,\theta)=Z_{-\infty}(\theta)+P_\infty\frac{Z_0(\theta)-Z_{-\infty}(\theta)}{P_\infty-p} \tag{6}$$

These linear fractional equations, also known as logistic equations, emphasize the nature of the Schemipflug geometry (Dremel et al 1996), that is, the limiting response ($R= R_{-\infty}$) for p as it approaches $-\infty$ (collection path parallel to the position detector) and ($p=P_\infty$) for R as it approaches $+\infty$ (projected ray parallel to collection path).

The coordinates of points D, E, and F are

$$X_{-\infty}(\theta)=-\frac{T\cos(\beta-2\theta)+S\cos(\beta)\sin(\gamma/2-\theta)}{\cos(\beta-\gamma)} \tag{7}$$

$$Z_{-\infty}(\theta)=\frac{T(\sin(\beta-2\theta)+\sin(\beta-\gamma))}{\cos(\beta-\gamma)}-\frac{S\cos(\beta)\cos(\gamma/2-\theta)}{\cos(\beta-\gamma)} \tag{8}$$

$$X_0(\theta)=-T\frac{\sin(2\theta)}{\sin(\gamma)} \tag{9}$$

$$Z_0(\theta) = T\frac{\cos(2\theta)+\cos(\gamma)}{\sin(\gamma)} \tag{10}$$

where S is the distance between the lens and the effective position of the collection axis pivot and T is the half distance between the projection and collection pivots. Those equations constitute the basis for the calibration algorithm.

3.3 Device Description

The developed auto-synchronized scanning laser device is shown in Figure 3-6.

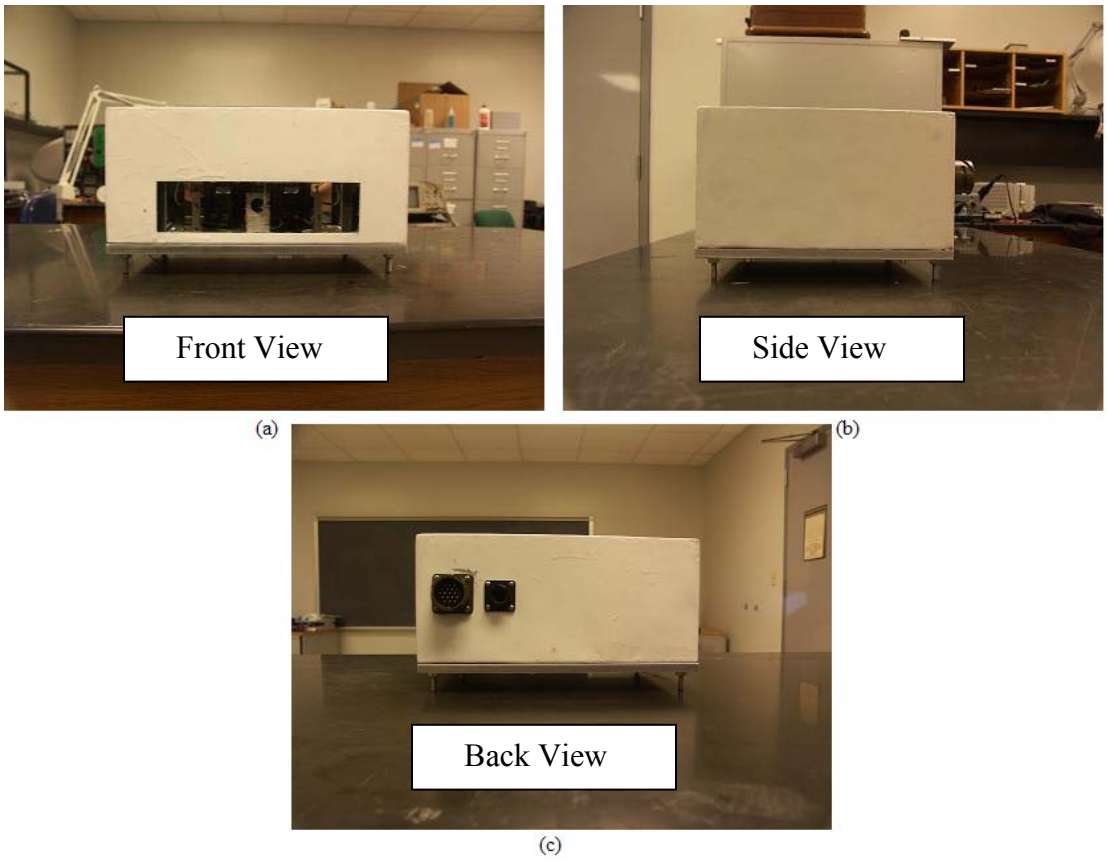

Figure 3-6 Laser Device Based on Auto-synchronized Scanning Principle

The physical dimensions of the laser device are 12 inches width, 10 inches depth and 5.75 inches height. The total weight is 12 lb.

The internal structure of the scanning laser device is shown in Figure 3-7. The device consists of a laser diode, scanning mirror, projection mirror, recollection mirror, lens, position sensitive detector, signal processing circuitry and power supply.

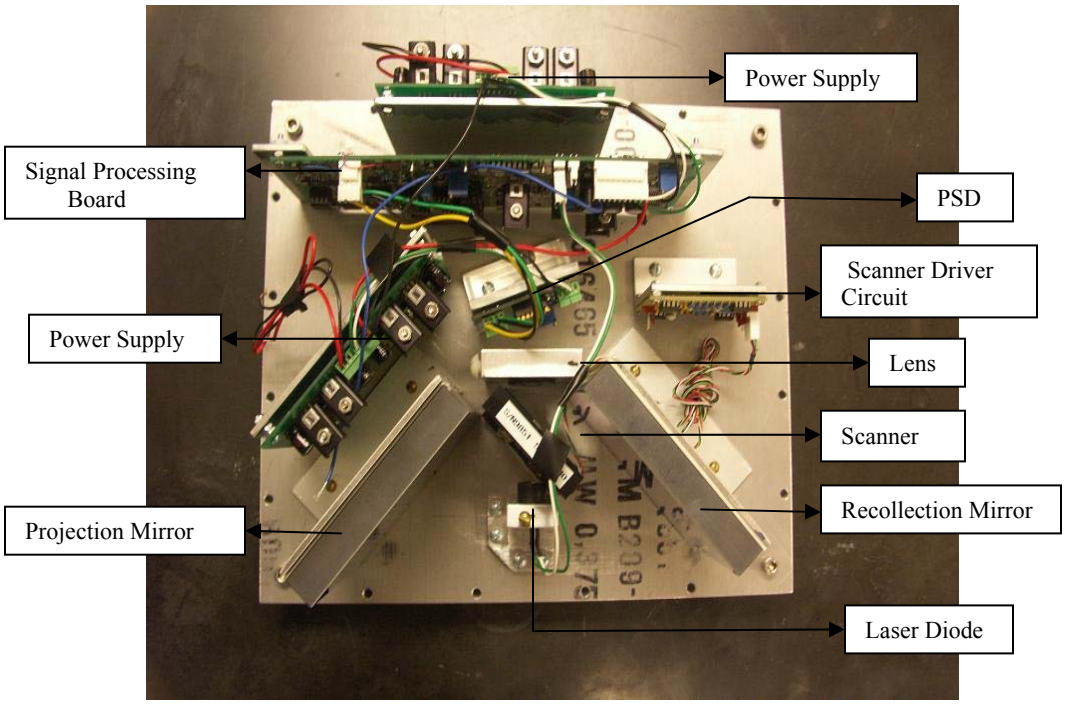

Figure 3-7 Internal Structure of the Scanning Laser Device

3.3.1 Optical specification

A 500mW He-Ne laser diode is used as the laser beam source. The wavelength of the laser diode is 808 nm which is near the sensitivity spectrum of the PSD sensor. The diode is placed in an optical holder which collimates the laser beam for the required measuring range. A double side mirror coated with enhanced aluminum on both sides is attached to a resonant scanner, which gives up to a 40° field of view (corresponding 12 inches width at standoff distance which is also 12 inches). A lens of 30mm focal length is used to focus the scattered light from the scene onto the PSD sensor. The PSD sensor is placed at a tilting angle β of 71.7° with the lens axis to comply with the Scheimpflug condition (Dremel et al 1996) in order to provide a considerable improvement in the depth of view without compromising the collected energy. Two same dimension single

side coated mirrors are used. The dimension of each one is 100mm (length) x 100 mm (height) x15 mm (thickness). One is used as projection directing and the other is used as reflection directing. Both of them are coated with enhanced aluminum.

To get rid of the optical noise from the sunshine, a laser bandpass filter is installed behind the lens. The bandpass filter also called as interference filter can transmit the laser of some specific wavelength and block other wavelength by using the light interference. Figure 3-8 shows the picture of the interference filter used in the auto-synchronized scanning laser device.

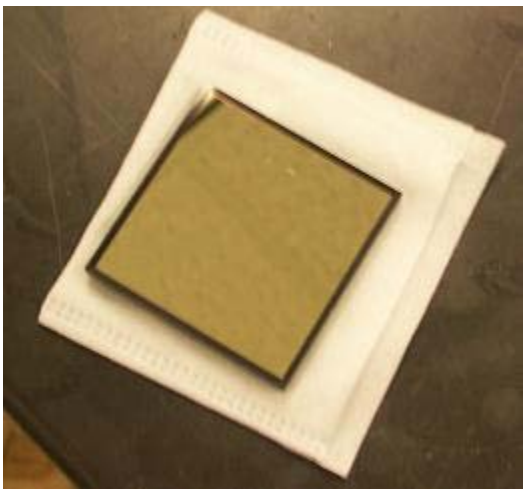

Figure 3-8 Laser Bandpass Filter

The dimension of this bandpass filter is 2.0 inches (length) x 2.0 inches (height) x 0.2 inch (thickness). The central wavelength is 800 nm, and the bandwidth is +/-10nm. The peak transmittance is above 50%. Figure 3-9 shows the transmittance chart of the bandpass filter.

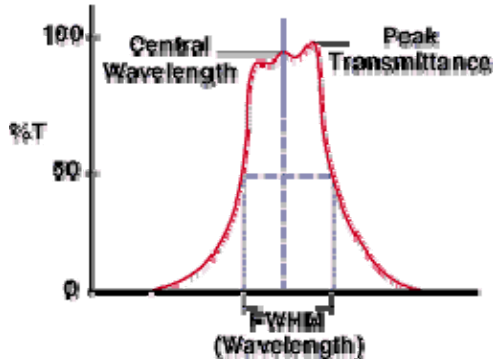

Figure 3-9 Transmittance Chart of the Bandpass filter

Figure 3-10 shows the output electronic signal of the system under the sunshine without installation of the bandpass filter.

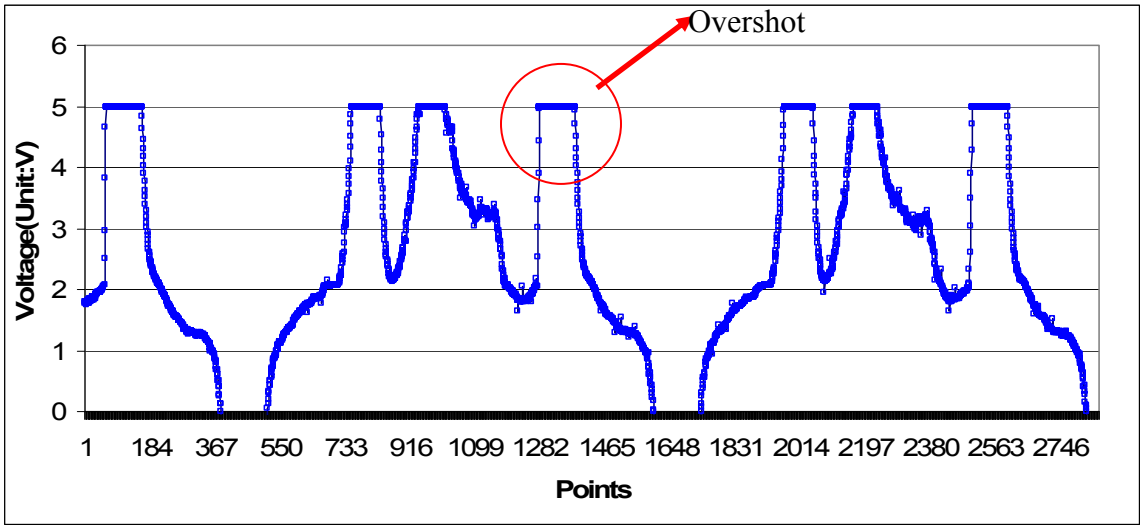

Figure 3-10 Output Electronic Signal Under Sunshine without Filter

Figure 3-11 shows the output electronic signal of the system under sunshine with the bandpass filter.

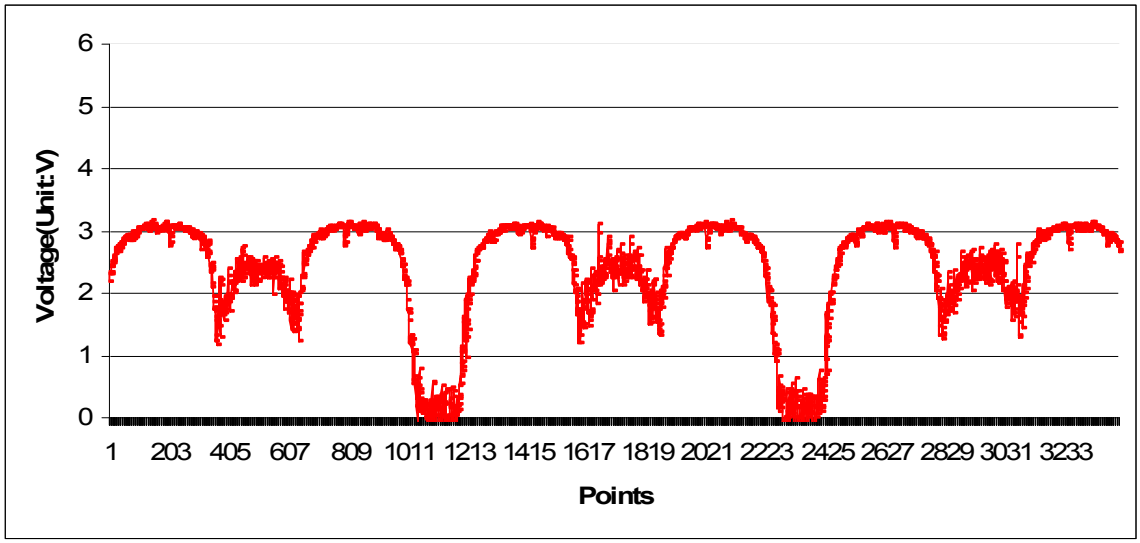

Figure 3-11 Output Electronic Signal under Sunshine with Bandpass Filter

From above two figures, we can see the bandpass filter can effectively remove the overshot signal which is caused by the sunshine.

3.3.2 Scanning laser system structure

To descript the architecture of the device, a simple hardware block diagram is depicted in Figure 3-12.

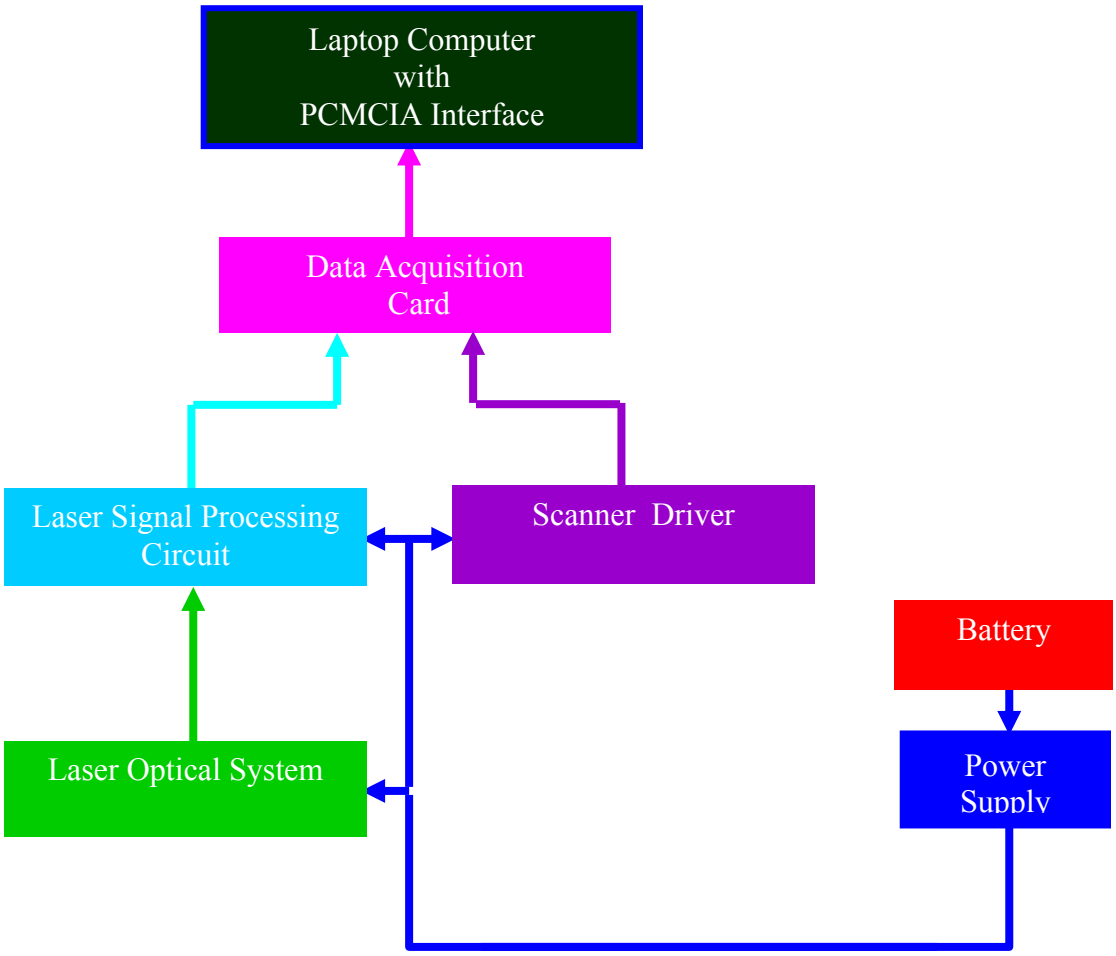

Figure 3-12 Block Diagram of Hardware

The prototype hardware of the pavement marking thickness measurement system based on the auto-synchronize laser scanning technique is composed of a laser optical subsystem, electronic processing and control subsystem, and power supply subsystem. The laser optical subsystem has been described before. The electronic processing and control subsystem consists of a laser signal processing circuit, scanning driver circuit and data acquisition. Only a 12 V DC power supply is necessary for the device. By using DC-DC voltage converters and voltage regulators, the 12 V output from the DC power supply is converted to + 15 V and +5 V, which is necessary for the laser electronic signal processing circuit.

Figure 3-13 is the scanning laser device is mounted on a frame for Lab test.

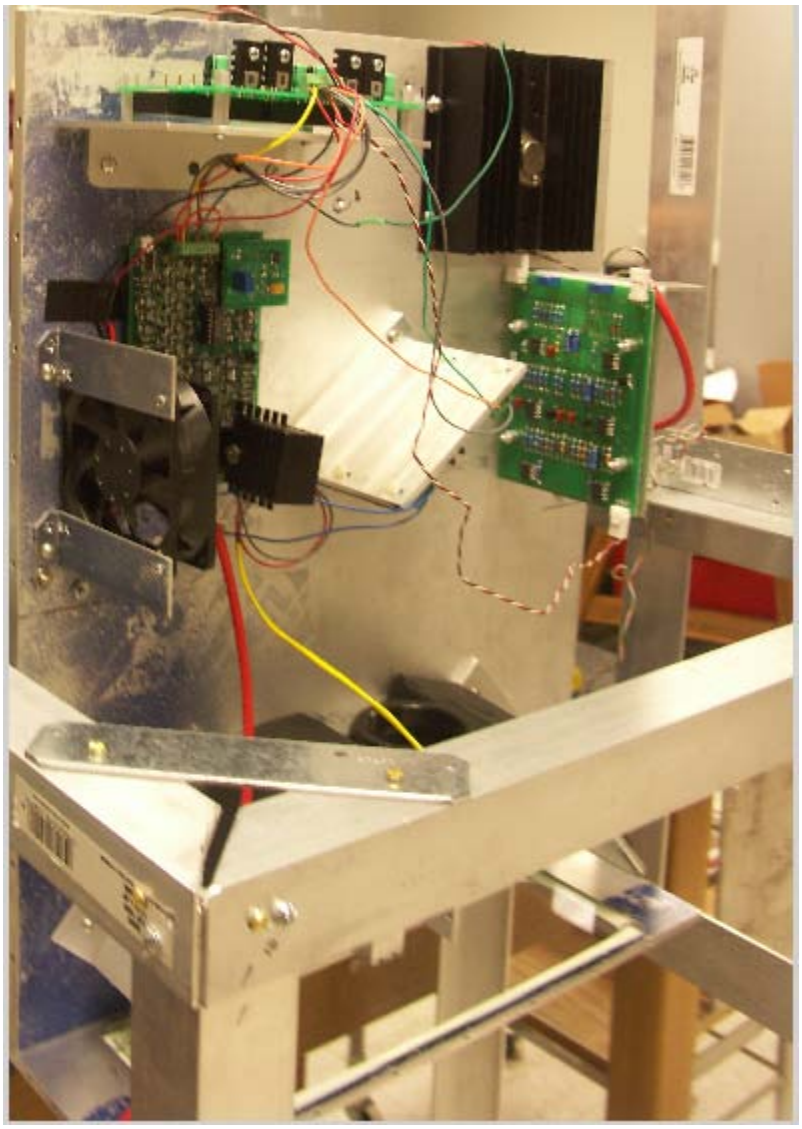

Figure 3-13 Scanning laser device mounted on a frame for Lab test

CHAPTER 4: LAB EXPERIMENTAL RESULTS

4.1 Scanning laser setup in the Lab

For Lab test, the scanning laser device is set up on an aluminum frame if Figure 4.1.

Figure 4-1 Scanning laser setup on a frame

To verify the accuracy the developed device, three asphalt samples have been built, a bare, a medium, and a flushed sample, as shown in Figure 4-2.

Figure 4-2 Test samples of bare, medium, and flushed asphalt slabs

The laser device is setup 80 cm above the test samples.

Figure 4-3 Experimental setup for sample testing

4.2 Calibration Using Wood Surface

To calibrate the device, a flat wood plank is used to do the testing first, as shown in Figure 4-4. The testing is repeated ten times, the results in Figure 4-5 demonstrate good repeatability. The measured curves should look a peak of a sinusoidal wave due to the laser-plank distance changing. The measured signals are very close to what expected. However, there is some interference from leaking laser beams, causing a dent on the top of the curves. This effect can be fixed either by sealing the leaking paths or by subtracting it from the laser signals.

Figure 4-4 Calibration using a flat plank

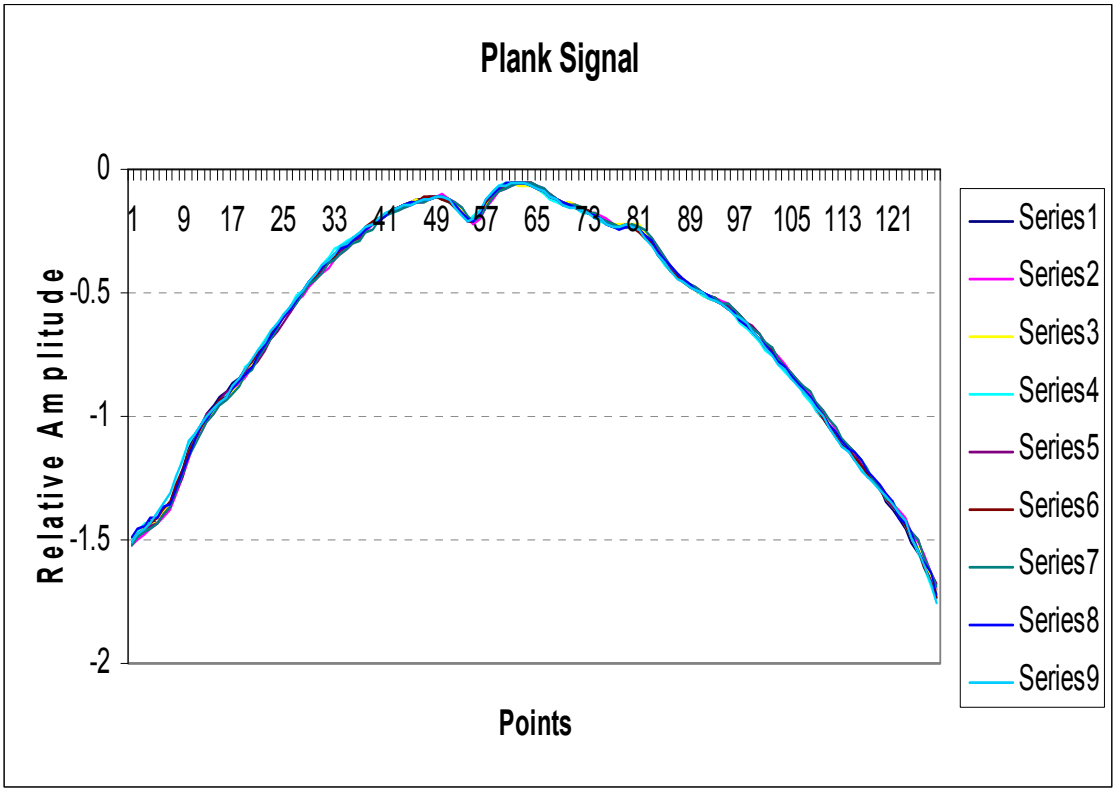

Figure 4-5 Measured laser signals over wood plank

4.3 Resolution Test

To test the device resolution, the wood plank is lifted 1 mm for each measurement by inserting 1 mm thick metal sheets under the plank as shown in Figure 4-6. From the measured waveforms in Figure 4.7, it can be seen that the waveforms neatly shift up accordingly. It's clear the device has a resolution higher than 1 mm.

Figure 4-6 wood plank is raised up 1 mm for each measurement by inserting metal sheets

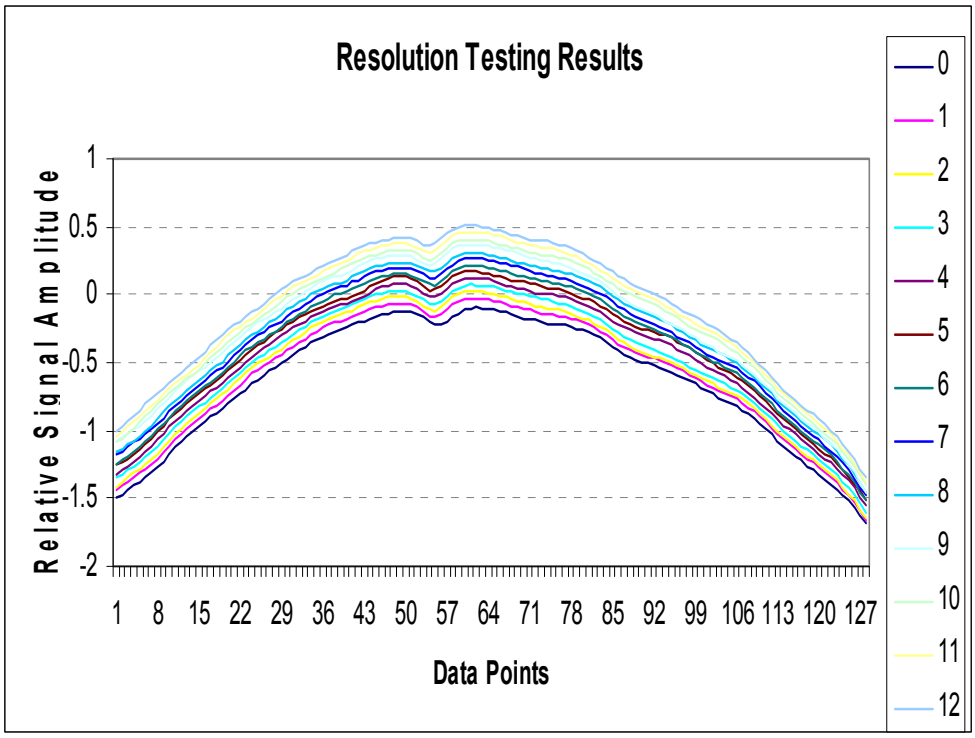

Figure 4-7 The measured waveforms shift upwards while plank is rising

4.4 Sample Tests

After the resolution test, the 3 asphalt samples are tested. Figure 4-8 show the results measured over the flushed asphalt sample. The laser beam is not exactly on the same line, the measured values are slightly changed for each measurement.

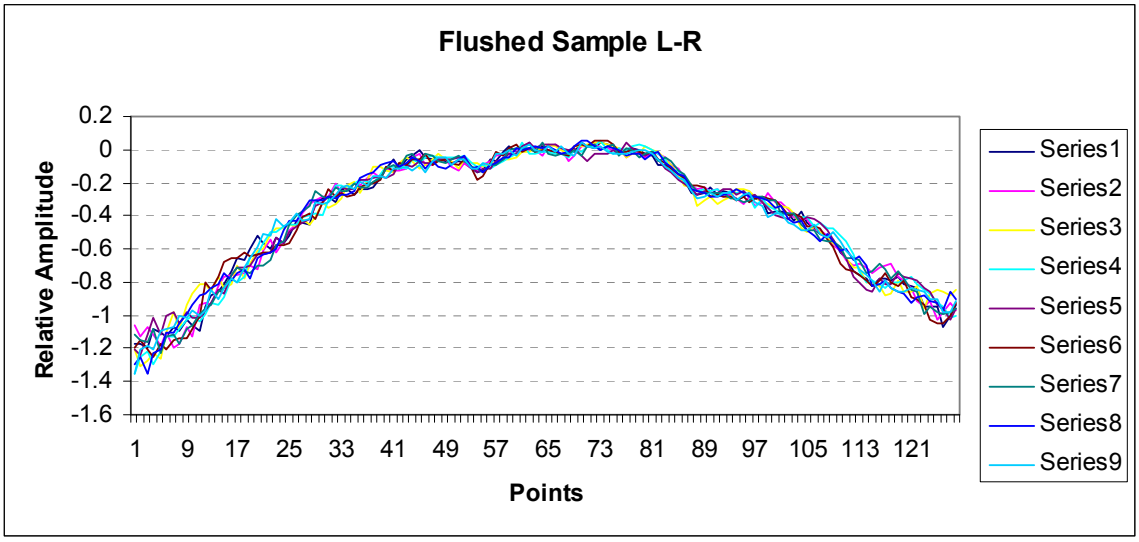

Figure 4-8 10 measurements carried out on the flushed sample

Figure 4-9 are the waveforms measured over the medium sample. We can see more humps popping out, which are profiles of little rocks.

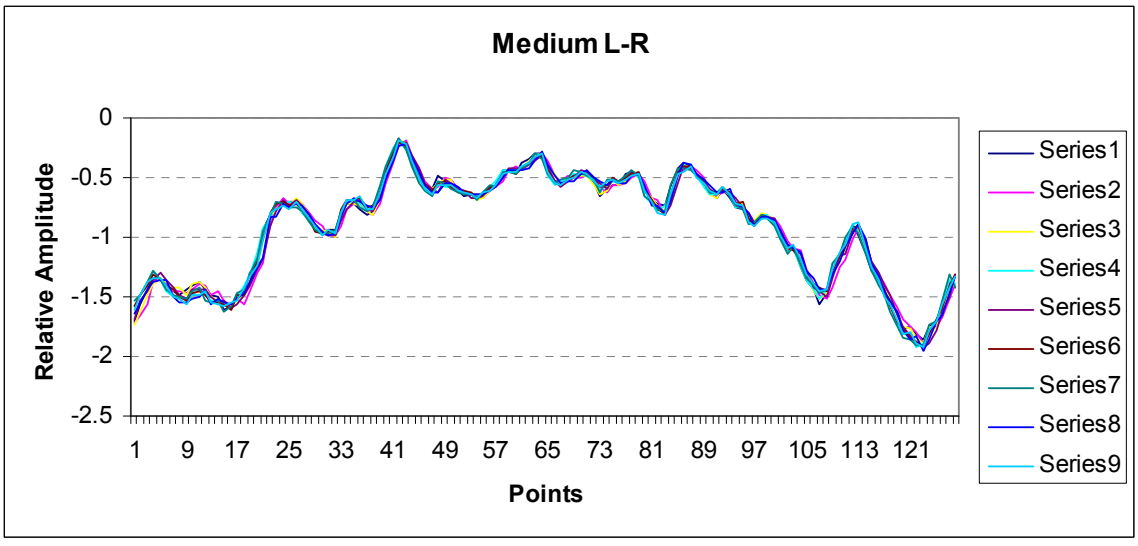

Figure 4-9 Measured waveforms over the medium sample

The waveforms measured over the flushed sample are shown in Figure 4-10. The curves do represent the profile of the bare asphalt pavement.

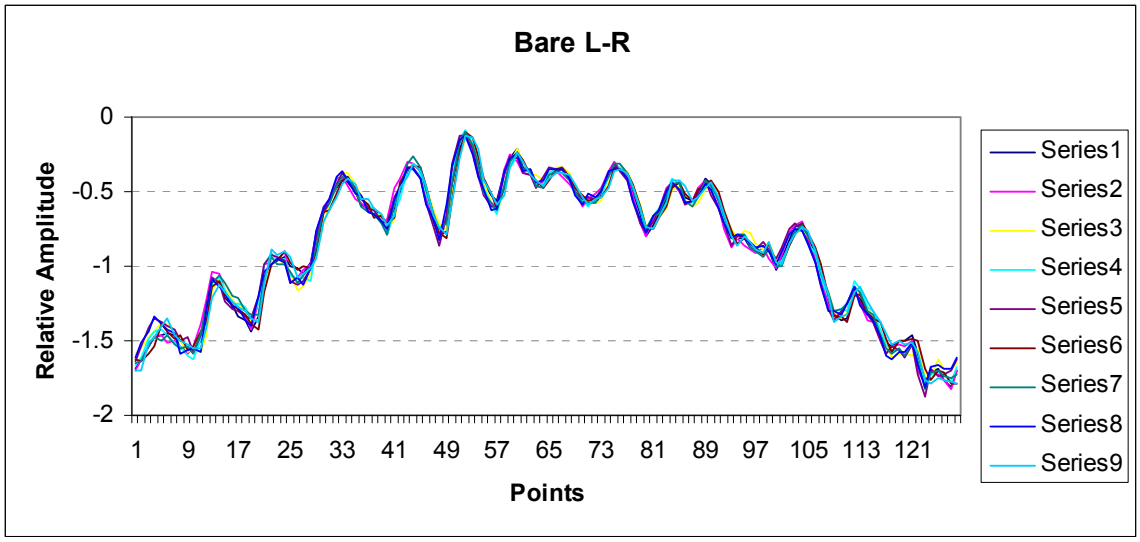

Figure 4-10 Measured waveforms over the medium sample

Comparing Figure 4-8, 4-9, and 4-10, it can be seen that the developed scanning laser device is able to tell the difference of the flushed, medium, and bare asphalt samples. By certain signal processing, the seal coat quality can be quantitatively described.

CHAPTER 5: CONCLUSIONS AND SUGGESTIONS

The 3-D laser scanning system based on auto-synchronized scanning is developed for seal coat quality evaluation. To achieve high-speed measurement, a PSD (Position Sensitive Detector) is used in the prototype system instead of a CCD (Charge Couple Device), which is usually used in the common imaging system. Compared to the previous mechanical scanning device, which gives two scan lines per second, the new system is more suitable for highway speed measurement. The system has been tested in Lab, and the results show that is device has a resolution higher than 1 millimeter with very good repeatability. The three sample testing results clearly show the profile features of flushed, bare, and medium asphalt pavements. By proper signal processing, the seal coat features can be quantitatively described.

Next step:

1. Software should be developed to convert the scanning laser's arch-shaped waveform to match the real flat pavement surface;
2. Laser device structure will be redesigned to prevent from laser leakage;
3. Field tests;
4. Establish criterion of seal coat quality factor

References:

Benson, F.J. and Galloway, B.M. (1953) Retention of Cover Stone by Asphalt Surface Treatments, Bulletin 133, Texas Engineering Experiment Station, Texas A&M University System.

Blais F., Rioux M., Beraldin J-A. (1988) Practical considerations for a design of a high precision 3-D laser scanner system, *Proc of the SPIE.*, Vol. 959, pp 225-246.

Brock, J. D., May, J. G., and Renegar, G., *Segregation Causes and Cure*s. *Technical Paper T-117*, Astec Industries, Chattanooga, Tenn., 1996.

Dremel, W., Häulser, G., and Maul M.(1996) Triangulation with a large dynamical range. *Proc. SPIE.,* 665, 182-187.

Holmgreen, R.J., Epps, J.A., Hughes, C.H. and Galloway, B.M. (1985) Field evaluation of the texas seal coat design method, Research Report 297-1F, Texas Transportation Institute, Texas A&M University System, College Station.

Janisch, D.W., and F.S. Gaillard. (1998). *Minnesota Seal Coat Handbook* . Report MN/RC-1999-07. Minnesota Local Road Research Board, Minnesota Department of Transportation, St. Paul, MN.

Manuel, C. F. M. (1996) Surface Inspection by an Optical Triangulation Method, *Opt. Eng*., 35(9), pp. 2743-2747.

Nicholas J. G., and Lester A. H., (1997). *Traffic and Highway Engineering*, 2nd Ed., PWS Publishing Co., New York.

Roadware Corporation, "Technical Reference Manual - Version 1.1," 1995.

Rioux, M. (1994) Laser range finder based on synchronized scanners, *Appl. Opt*., 23(21), pp. 3837-3844.

Rioux, M., and Bechtold, G., Taylor, D., and Duggan, M., (1987). Design of a large depth of view three-dimensional camera for robot vision, *Opt Eng.,* 26(12), pp. 1245-1250.

Wiese, D. R., (1989) Laser Triangulation Sensors: A Good Choice for High Speed Inspection, *Chilton's I&CS (Instrumentation and Control System)*, 62, pp, 27-29.